Biosensors and Bioelectronics 155 (2020) 112106

Contents lists available at ScienceDirect

Biosensors and Bioelectronics

journal homepage: http://www.elsevier.com/locate/bios

Gd^{3+}-nanoparticle-enhanced multivalent biosensing that combines magnetic relaxation switching and magnetic separation

Yunlei Xianyu [b,c,d,1], Yongzhen Dong [a,e,1], Zhuo Zhang [a,e], Zhanhui Wang [f], Wenbo Yu [f], Zhilong Wang [a,e], Yiping Chen [a,e,*]

[a] College of Food Science and Technology, Huazhong Agricultural University, Wuhan, 430070, Hubei, China
[b] College of Biosystems Engineering and Food Science, Zhejiang University, Hangzhou, 310058, Zhejiang, China
[c] Fuli Institute of Food Science, Zhejiang University, Hangzhou, 310058, Zhejiang, China
[d] Ningbo Research Institute, Zhejiang University, Ningbo, 315100, Zhejiang, China
[e] Key Laboratory of Environment Correlative Dietology, Huazhong Agricultural University, Ministry of Education, Wuhan, China
[f] Beijing Advanced Innovation Center for Food Nutrition and Human Health, College of Veterinary Medicine, China Agricultural University, Beijing Key Laboratory of Detection Technology for Animal-Derived Food Safety, and Beijing Laboratory for Food Quality and Safety, Beijing, 100193, China

ARTICLE INFO

Keywords:
Gd^{3+}-nanoparticle
Multivalent magnetic probe
Magnetic relaxation switching
Biosensing

ABSTRACT

In this work, we developed a multivalent magnetic biosensing strategy by integrating magnetic separation and magnetic relaxation switching (MRS) where Gd^{3+}-loaded magnetic nanoparticles acted as the probe. As a transition metal ion, Gd^{3+} has multiple unpaired electrons in the d-orbitals that can induce a strong fluctuating magnetic field and thus can reduce the transverse relaxation time (T_2), contributing to a strong magnetic signal. By loading Gd^{3+} onto magnetic nanoparticles, we prepared a multivalent magnetic probe that combined magnetic separation and MRS for the signal readout. This multivalent sensing technique simplified the procedures and greatly enhanced the detection sensitivity of conventional MRS assays. A sensitive detection of ractopamine in real samples has been demonstrated with this multivalent sensing technique. The magnetic probe enabled the detection of ractopamine in a linear range from 0.1 to 100 ng/mL and the limit of detection was 20 pg/mL, a 25-fold enhancement in the sensitivity compared with conventional MRS assays. This Gd^{3+}-nanoparticle-mediated MRS biosensor is a potential magnetic platform to detect trace levels of targets in complex samples.

1. Introduction

Magnetic biosensors have been extensively researched in both *in-vitro* diagnosis and *in vivo* imaging (Haun et al., 2010; Huber et al., 2019; Lei et al., 2018; Ma et al., 2013; Xu et al., 2012; Zhang et al., 2019). For *in-vitro* diagnosis, magnetic particles such as iron oxides are widely used in biosensors owing to their extraordinary features such as the straightforward magnetic separation, the extraordinary magnetic signals, the versatile surface modification, and the good stability (Chen et al., 2013; Chung et al., 2013; Kang et al., 2017; Shao et al., 2012; Srinivasan et al., 2018; Wang et al., 2018b; Xianyu et al., 2018; Xiao et al., 2018; Yang et al., 2018; Zhang and Zhou, 2012). For *in vivo* applications such as the magnetic resonance imaging, contrast agents such as Gd^{3+}-based chelates have been widely employed in both laboratory research and real clinic due to the long electron spin relaxation time of Gd^{3+} (Caravan, 2006; Caravan et al., 1999; Ni et al., 2017; Shin et al., 2018; Wang et al., 2018a; Zhang et al., 2018; Zhou et al., 2017). Gd^{3+}-based chelates have shown as excellent candidates that can modulate the magnetic relaxation time in the magnetic resonance imaging (De Leon-Rodriguez et al., 2015; Rammohan et al., 2016; Zhao et al., 2018). The integration of magnetic separation and magnetic relaxation switching (MRS) into one biosensor is fascinating since it can enable the *in-vitro* diagnosis with great simplicity and high stability. To address this issue, we have reported an approach using 250 nm magnetic nanoparticles (MNPs) as the magnetic separation probe and 30 nm MNPs as the MRS probe for readout (Chen et al., 2015). The molecular event such as the antibody-antigen interaction induces the attachment of the small MRS probe on the large magnetic beads, leading to a signal change in the transverse relaxation time. The combination of MNPs of different sizes can simplify the procedures for the detection of

* Corresponding author. Key Laboratory of Environment Correlative Dietology, Huazhong Agricultural University, Ministry of Education, Wuhan, China.
E-mail address: chenyiping@mail.hzau.edu.cn (Y. Chen).
[1] These authors contribute to this manuscript equally.

https://doi.org/10.1016/j.bios.2020.112106
Received 2 November 2019; Received in revised form 7 January 2020; Accepted 17 February 2020
Available online 19 February 2020
0956-5663/© 2020 Elsevier B.V. All rights reserved.

biomacromolecules, but it is not competent to detect small molecules such as the antibiotics because of the low sensitivity. The bottleneck of this approach is the insufficient number of 30 nm MNPs attached for the readout that cannot achieve the high sensitivity required for small molecule detection.

The limited sensitivity in conventional nanoparticles-based method is due to the lack of enough MRS signal probes. Given that Gd^{3+}-based chelates have been widely used as contrast agents to modulate the magnetic relaxation time in the magnetic resonance imaging, it would be beneficial to employ Gd^{3+}-based chelates as signal probes in the MRS bioassays. As a transition metal ion, Gd^{3+} can play as a signal probe for the MRS assay. Gd^{3+} has multiple unpaired electrons in the d-orbitals able to induce a strong fluctuating magnetic field and thus shorten the magnetic relaxation time. Compared with MNPs, the size of metal ions is much smaller that is beneficial for improving the sensitivity to achieve the small molecule detection with high sensitivity (Wu et al., 2018). Therefore, the integration of paramagnetic ions and MNPs could be an attractive strategy to prepare multivalent magnetic probes that can enhance the sensitivity of traditional magnetic biosensors.

To address the issue of low sensitivity, in this study we prepare a magnetic probe composing of 150 nm MNPs (MNP_{150}) and Gd^{3+}-based chelates that are expected to significantly improve the magnetic relaxation property of conventional probes, thus allowing for an enhanced sensitivity for biosensing applications (eMRS). Using the coordination chemistry between Gd^{3+} and chelators such as 1,4,7,10-tetraazacyclododecane-1,4,7,10-tetraacetic acid (DOTA), Gd^{3+} can be anchored on DOTA to form gadoteric acid that can dramatically reduce the longitudinal relaxation time (T_1) or the transverse relaxation time (T_2) contributing to an enhanced MRS signal (Bryant et al., 1999; Cao et al., 2014). In addition, the combination of Gd^{3+}-based chelates and MNP_{150} can endow the assay with features in both the magnetic separation and an MRS readout. On one hand, upon the implementation and removal of a magnetic field, it enables the manipulation of the MNPs. The magnetic separation feature allows a facile purification that can decrease the matrix effect in complex settings. On the other hand, Gd^{3+}-based chelates have excellent MRS signals that can act as signal amplifiers to modulate the T_1 and T_2 signals in the biosensors for an enhanced sensitivity. By combing MNPs and the coordination chemistry between Gd^{3+} and DOTA, we developed an eMRS technique that can enable both a straightforward magnetic separation and a highly sensitive MRS readout (Scheme 1). Ractopamine as a beta-agonist drug has been prohibited in breeding industry, and detecting the presence of ractopamine can ensure human health (Baynes et al., 2016). For proof of concept, we employ this eMRS for the highly sensitive and rapid detection of ractopamine, showing its potential as a sensitive and rapid detection technique for magnetic bioassays.

2. Experimental section

2.1. Preparation of antibody (Ab)-MNP_{150}-polylysine conjugate

20 μL of EDC (10 mg/mL) and 10 μL of NHS (10 mg/mL) were mixed with the Ab solution (100 μL, 2.5 mg/mL), and this mixture was shaken for 10 min at room temperature. 500 μL of NH_2-MNP_{150} (2 mg/mL) was mixed with the solution above and was gently shaken for 1 h at room temperature. After magnetic separation, 500 μL of PBS solution (0.01 M, pH = 7.4) was used to resuspend the Ab-MNP_{150} conjugate. Polylysine solution (10 μL, 20 mg/mL) was further added into the Ab-MNP_{150} conjugate solution and the mixture was incubated for 1.5 h. After the magnetic separation and washing, 1000 μL of PBS was added to resuspend the Ab-MNP_{150}-polylysine conjugate (1 mg/mL).

2.2. Preparation of Ab-MNP_{150}-polylysine-DOTA conjugate

100 μL of DOTA-NHS ester (200 μM) was added into the above Ab-MNP_{150}-polylysine conjugate solution, and the solution was mildly stirred for 2 h at room temperature. After magnetically separated and washed for twice, the Ab-MNP_{150}-polylysine-DOTA conjugate (2 mg/mL) was resuspended by using 500 μL of deionized water. The conjugte was stored at 4 °C for further use.

2.3. Preparation of Ab-MNP_{150}-polylysine-DOTA-Gd^{3+} conjugate

250 μL of Gd^{3+} solution (400 μM) was mixed with 500 μL of the Ab-MNP_{150}-polylysine-DOTA conjugate (2 mg/mL). The mixture was gently stirred for 4 h at room temperature. After the magnetic separation and washing for twice with deionized water, the Ab-MNP_{150}-polylysine-DOTA-Gd^{3+} probe (1 mg/mL) was resuspended using 1000 μL of PBS. The conjugate was further used for the T_2 readout by a 0.47T NMR instrument (PQ001).

2.4. The eMRS based on Ab-MNP_{150}-polylysine-DOTA-Gd^{3+} probe

100 μL of the complete antigen (BSA-ractopamine, 50 μg/mL) diluted in 0.01 M carbonate buffer solution (pH = 9.6) was coated on the ELISA plate and incubated at 37 °C for 2 h. After washing with PBST (PBS with additional 0.05% Tween-20, 0.01 M, pH = 7.4) for three times, 100 μL of Ab-MNP_{150}-polylysine-DOTA-Gd^{3+} probe (100 μg/mL)

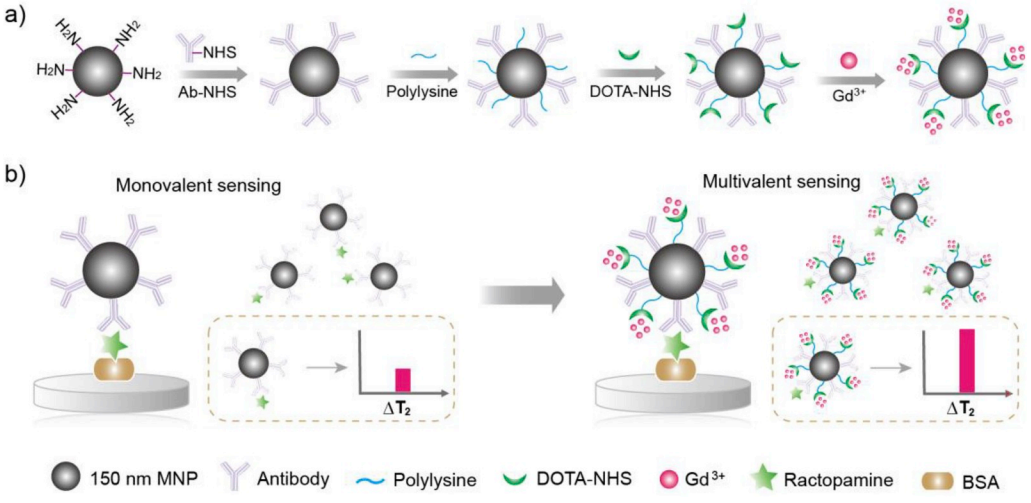

Scheme 1. Schematic illustration of **a**) the preparation of Gd^{3+}-nanoparticle-mediated multivalent magnetic probe and **b**) magnetic relaxation switching bioassays of ractopamine using the multivalent magnetic probe.

was added into a range of concentrations of ractopamine (1000, 500, 100, 50, 10, 5, 1, 0.5, 0.1, 0.05, 0.001, and 0 ng/mL), respectively. This mixture was shaken at 37 °C for 15 min. After that, the Ab-MNP_{150}-polylysine-DOTA-Gd^{3+} probes were magnetically separated and were further added into the ELISA plate to react with the complete antigen (BSA-ractopamine). The ELISA plate was gently shaken at room temperature for 30 min, followed by washing with PBST (0.05% Tween-20) for three times to remove the non-reacted Ab-MNP_{150}-polylysine-DOTA-Gd^{3+} probes. 200 μL of PBST (5% Tween-20) was further added to the ELISA plate for 3 min to dissociate the immuno-complex between BSA-ractopamine and Ab-MNP_{150}-polylysine-DOTA-Gd^{3+}. The dissociated Ab-MNP_{150}-polylysine-DOTA-Gd^{3+} in the solution was finally collected to obtain the T_2 signal.

2.5. Calculation of the number of Gd^{3+} conjugated on one MNP_{150}

The number of Gd^{3+} conjugated to one MNP_{150} was calculated as follows. First, the BCA kit was used to quantify the amount of polylysine on the surface of MNP_{150} (Fig. S3). Based on the quantification result, it was concluded that 1 mg of MNP_{150} can conjugate 195.9 μg of polylysine. Given that the average molecular weight of polylysine is 50 kDa, the number of polylysine molecules conjugated on 1 mg MNP_{150} is calculated to be 2.358×10^{15}. Since 1 mg MNP_{150} contain 5×10^{10} nanoaprticles, the number of polylysine molecules conjugated on one MNP_{150} is about 4.72×10^{4}. One polylysine molecule has around 390 $-NH_2$ groups that can be further conjugated with NHS-DOTA and Gd^{3+}, thus the number of Gd^{3+} conjugated on one MNP_{150} is calculated to be $390\times4.72\times10^{4} = 1.84\times10^{7}$.

2.6. The ELISA procedures for detection of ractopamine

The process for coating the complete antigen was the same as the section 2.4. After washing with PBST for three times, 50 μL of Ab solution (5 μg/mL) and 50 μL of different concentrations of ractopamine (1000, 500, 100, 50, 10, 5, 1, 0.5, 0.1, 0.05, 0.001, and 0 ng/mL) were mixed, respectively. The mixture was gently added into the ELISA plate coated with the complete antigen, and was gently shaken at room temperature for 2 h. This ELISA plate was washed with PBST (0.05% Tween-20) for three times. Then 100 μL of HRP-labelled sheep anti-mouse secondary antibody (0.5 μg/mL) was added into the ELISA plate for 1 h. After washing for four times with PBST, 50 μL of tetramethylbenzidine was added into the ELISA plate. After reaction for 5 min, 50 μL of H_2SO_4 (2 M) was added into the plate to terminate the enzymatic reaction. The microplate reader was used to obtain the OD_{450} value.

2.7. Detection of ractopamine in swine urine samples

Swine urine samples were provided by the College of Animal Science and Technology, Huazhong Agricultural University. These swine urine samples were 5-fold diluted by PBS solution, and were detected by eMRS and ELISA. The results of HPLC-MS for ractopamine detection were provided by Chinese Academy of Inspection and Quarantine (Beijing, China).

3. Results and discussion

3.1. Gd^{3+}-DOTA as the magnetic signal probe

Gd^{3+}-based chelates enable the shortening of the magnetic relaxation time of surrounding water protons for an enhanced sensitivity. Based on the Solomon–Bloembergen–Morgen theory, there are several ways to enhance the magnetic relaxation signals such as using a long rotational correlation time and an optimized water residence time, as well as increased bound water molecules (Zhou et al., 2019). A number of approaches have been reported to modulate these parameters to achieve a high relaxivity by introducing nanoparticles and controlling their size, shape, morphology and surface chemistry (Ananta et al., 2010; Rotz et al., 2015; Zheng et al., 2017). One widely employed way to enhance the relaxivity is to dock multiple Gd^{3+}-based chelates onto nanoparticles to increase the number of paramagnetic centers per unit (Marangoni et al., 2017; Wang et al., 2017). The docking of Gd^{3+} has two advantages. First, it can slow down the tumbling motion to make the magnetic center better fit the Lar mor frequency. Secondly, it enables an optimized water residence time and increased bound water molecules (Zhang et al., 2018). With this strategy, Gd^{3+}-based chelates functionalized on nanoparticles can effectively play as excellent MRS probes for *in vitro* biosensing. In this work, we employed the coordination chemistry between Gd^{3+} and DOTA to prepare Gd^{3+}-DOTA chelates. The multivalent magnetic probe is made by conjugating DOTA onto MNP_{150} to form a nanoparticle-core DOTA-shell nanostructure for Gd^{3+} coordination. Considering that multiple DOTA molecules can be conjugated onto each nanoparticle, the large Gd^{3} -loading capacity of the nanostructure is expected to dramatically amplify the magnetic signal for an enhanced sensitivity.

3.2. Synthesis and characterization of MNPs-DOTA-Gd^{3+} nanostructure

We prepared the multivalent magnetic probe by using MNPs of 150 nm functionalized with antibody and polylysine. Amine-terminated MNPs were first conjugated with NHS-antibody through EDC/NHS chemistry, and were further blocked by polylysine for the conjugation of DOTA. Amine groups on polylysine can react with NHS-DOTA through EDC/NHS chemistry. We optimized the ratio between the polylysine-modified MNPs and DOTA to prepare the MNPs-DOTA conjugate, followed by the introduction of Gd^{3+} to form the MNPs-DOTA-Gd^{3+} nanostructure (Fig. S1). We characterized the step-by-step conjugation process by scanning electron microscopy (SEM), energy-dispersive spectrometry (EDS), and dynamic light scattering (DLS). The native MNPs showed a rough surface that became smooth after conjugation with DOTA and Gd^{3+} (Fig. 1A, D and 1G). Other than the morphological change, we employed energy dispersive spectrum-SEM (EDS-SEM) to analyze the elemental compositions before and after conjugation (Fig. 1B, E and 1H). The elemental analyses showed that after conjugation with DOTA, it showed a decreased percentage of Fe and an enhanced percentage of N, suggesting the successful modification of polylysine and DOTA. The weight percentage of N element in the MNPs-DOTA complex was measured to be 2.26%, suggesting that there were many molecules of polylysine and DOTA on the surface (Fig. 1C and F). After chelation with Gd^{3+}, the elemental Gd could be detected that suggested the successful preparation of MNPs-DOTA-Gd^{3+}. The weight percentage of Gd element in the MNPs-DOTA-Gd^{3+} complex was measured to be 0.39% (Fig. 1I). We also employed DLS to characterize the different conjugates. According to the size distribution results, the sizes of MNP_{150}, MNP_{150}-Ab, MNP_{150}-Ab-polylysine and MNPs-Ab-polylysine–DOTA-Gd^{3+} were 212.7 nm, 240.6 nm, 262.9 and 277.9 nm, respectively (Fig. 1J). The gradually increased size of MNPs suggested that both polylysine and DOTA were successfully conjugated onto the surface of MNPs. In addition, the zeta potentials of the MNP_{150}, Ab-MNP_{150}, MNP_{150}-Ab-polylysine-DOTA, and MNP_{150}-Ab-polylysine-DOTA-Gd^{3+} conjugate also changed from -35 mV to 10.5 mV (Fig. 1K).

3.3. Capacity of MNPs for the signal enhancement

In this work, we found that MNPs of 150 nm can function as a probe for both separation and readout. The MRS property of magnetic particles relates to the size of MNPs. Our previous study showed that 1000 nm MNPs enable magnetic separation under a given magnetic field and 30 nm MNPs can act as an MRS probe for the readout of bioassays. In this study, we investigated the MRS features of MNPs of different sizes including 150 nm, 250 nm, and 1000 nm. The results showed that 150 nm MNPs can play as an MRS probe because of the higher ability of 150

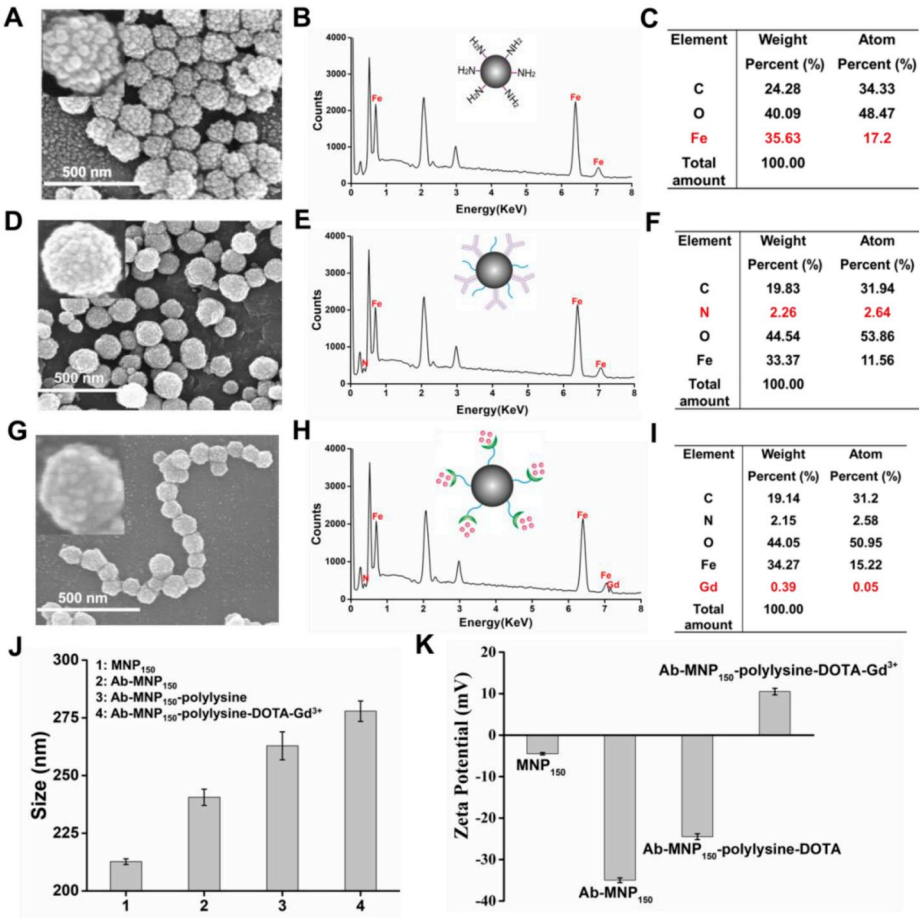

Fig. 1. Synthesis and characterizations of the MNPs-DOTA-Gd^{3+} nanostructure. **(A)–(I)** SEM images, EDS spectra and the elemental compositions of **(A)–(C)** MNP_{150}, **(D)–(F)** Ab-MNP_{150}-polylysine conjugate, and **(G)–(I)** Ab-MNP_{150}-polylysine-DOTA-Gd^{3+} nanostructure; **(J)** The size change and **(K)** the zeta potential of MNP_{150}, Ab-MNP_{150}, Ab-MNP_{150}-polylysine-DOTA conjugate and Ab-MNP_{150}-polylysine-DOTA-Gd^{3+} nanostructure.

nm MNPs to change the T_2 value and a better suspension stability than those of 250 nm MNPs and 1000 nm MNPs (Fig. 2A). As the concentration of MNPs increased, there was an increase in the change of the T_2 value. Apart from the MRS signal, the 150 nm MNPs are able to respond to a magnetic field and aggregate upon the introduction of a certain magnetic field. Unlike MNPs, Gd^{3+}-based chelates themselves only have MRS signals and they show no response under a magnetic field. The combination of magnetic separation and MRS can become useful for developing biosensors that can great simplify the assaying process and simultaneously have a straightforward readout. In this assay, the MNP core can be exploited to magnetically separate the versatile probe that can simplify the procedures. The shell of DOTA-Gd^{3+} chelates can be further used to generate significant T_2 signals for the readout. The core-shell nanostructure can be an excellent biosensing probe that fulfills both the magnetic separation and an MRS readout.

Prior to incorporating the DOTA-Gd^{3+} onto MNPs, we found that the DOTA-Gd^{3+} conjugate that has been widely used as a T_1 contrast generated a remarkable T_2 signal (Fig. S2), demonstrating that the incorporation of DOTA-Gd^{3+} into the multivalent magnetic probe could be beneficial for an enhanced T_2 signal. After the introduction of DOTA-Gd^{3+}, we compared the T_2 relaxivity of MNPs and the MNPs-DOTA-Gd^{3+}. Under the same molar concentration of MNPs, the MNPs-DOTA-Gd^{3+} showed a much higher T_2 relaxivity than the unmodified MNPs, demonstrating the effectiveness of the DOTA-Gd^{3+} for the signal enhancement (Fig. 2B). We also used the magnetic resonance imaging to characterize the MNPs-DOTA-Gd^{3+}. The image directly showed the magnetic signal intensity of the MNPs modified with different ligands and Gd^{3+} (Fig. 2C, D, and 2E). We calculated the amount of DOTA and Gd^{3+} conjugated on the surface of MNPs based on the quantification of amine groups on the MNPs (Fig. S3). NHS-antibody and polylysine were firstly conjugated on the surface of NH_2-MNP_{150}, followed by the introduction of DOTA-NHS ester to the surface of Ab-MNP_{150}-polylysine conjugate. Gd^{3+} ions were added into the above conjugate and DOTA could specifically bind Gd^{3+} ions due to the chelation between the carboxyl group and Gd^{3+}. The loaded amount of Gd^{3+} on one nanoparticle was calculated to be 1.84×10^7. The high loading capacity of Gd^{3+} owes to the large surface area of MNPs and the coordination chemistry between DOTA and Gd^{3+}, which makes it possible for the magnetic sensing with a high sensitivity.

3.4. eMRS for detection of ractopamine

We first used the MNPs of 150 nm for the assay because MNPs can be used as MRS probes to generate a T_2 signal. Other than the T_2 signal, MNPs can move under a magnetic field that can be used for separation. Using MNPs for magnetic separation and magnetic readout, we implemented a competitive immunoassay to detect ractopamine. Ractopamine as a feed additive poses threat to human health, and its detection is important for food safety. In this competitive assay, the BSA-ractopamine antigen was coated on the well plate. Upon the addition of the target small molecule, it would competitively bind with the antibody conjugated on the MNPs. The bound MNPs on the plate could then be employed for the magnetic readout of the immunoassays. The results showed that it enabled the detection of ractopamine when 150 nm MNPs were used, but it had insufficient sensitivity to detect the small molecule (Fig. 3A).

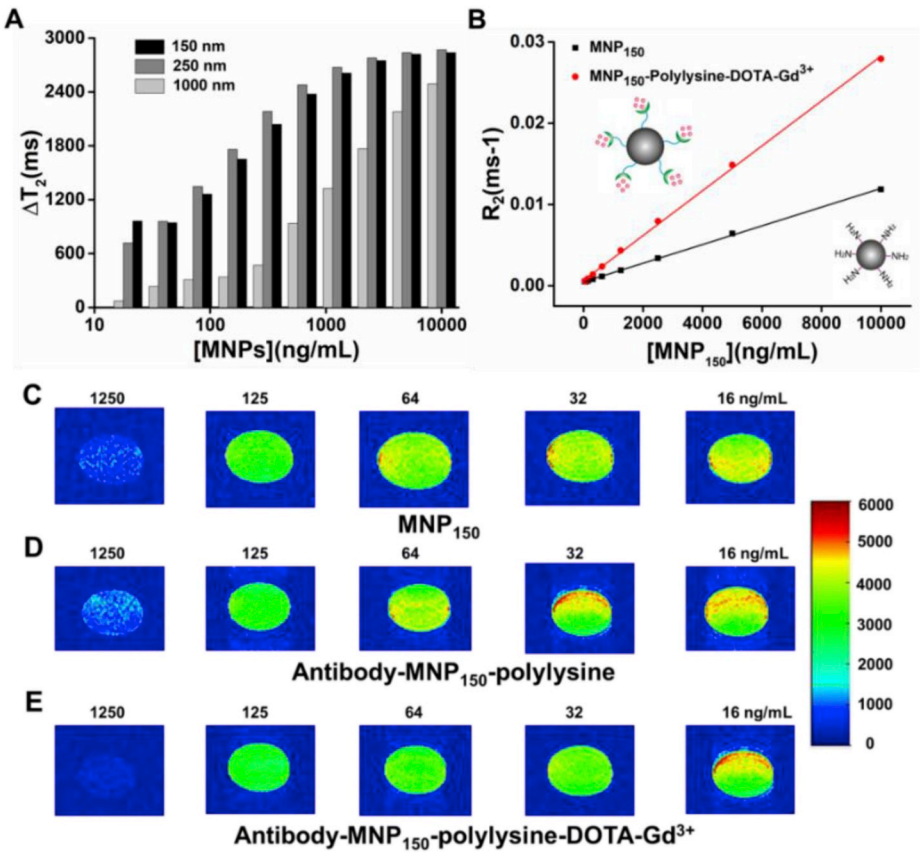

Fig. 2. Investigation of the magnetic relaxation property of MNPs and the Gd^{3+}-MNPs conjugate. **(A)** A comparison of the magnetic relaxation property of 150 nm MNPs, 250 nm MNPs and 1000 nm MNPs; **(B)** A comparison of transverse relaxation rate (R_2) of MNP_{150} and MNP_{150}-polylysine-DOTA-Gd^{3+}; **(C)**–**(E)** A comparison of magnetic resonance imaging between MNP_{150}, antibody-MNP_{150}-polylysine and antibody-MNP_{150}-polylysine-DOTA-Gd^{3+}, and the concentrations of the magnetic probes are 16, 32, 64, 125, and 1250 ng/mL. The units associated with the scale are millisecond (ms), representing the T_2 value.

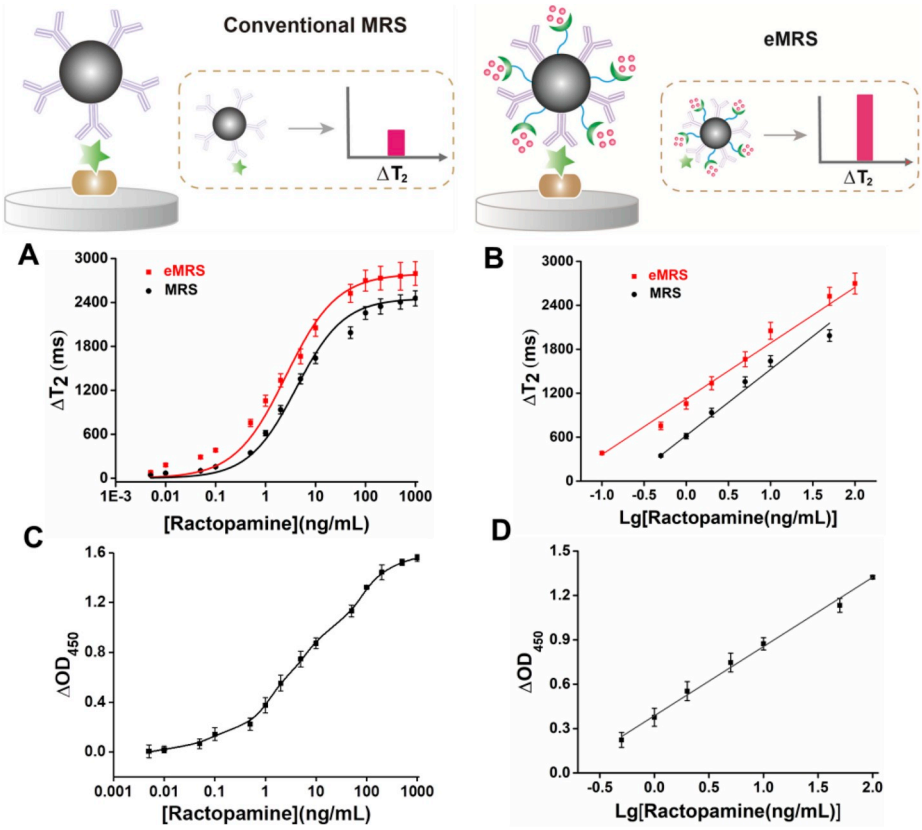

Fig. 3. Sensitivity and linear detection range of the eMRS, conventional MRS and ELISA for detection of ractopamine. **(A)** The standard curve of eMRS and conventional MRS for detection of ractopamine; **(B)** The linear range of the eMRS and conventional MRS for detection of ractopamine; **(C)** The standard curve of conventional ELISA for detection of ractopamine; **(D)** The linear range of conventional ELISA for detection of ractopamine. For the calculation of error bars, three samples were measured.

To achieve a higher sensitivity, we employed the MNPs-DOTA-Gd^{3+} as the magnetic probe for eMRS. We investigated and compared the sensitivities using MNPs and MNPs-DOTA-Gd^{3+} for detection of ractopamine. We optimized the conditions for the reaction and chose 100 μg/mL for the immunoassay (Fig. S4). The results showed that the ΔT_2 value had a concentration-dependent manner with ractopamine. The ΔT_2 value increased from 80 ms to 2795 ms when the concentration of ractopamine increased from 0.05 to 100 ng/mL. The linear range of eMRS for detection of ractopamine was from 0.1 to 100 ng/mL ($Y = 761X+1123$, $R^2 = 0.99$, X = lg[ractopamine]), broader than conventional MRS (from 0.5 to 100 ng/mL, $Y = 902X+622$, $R^2 = 0.99$, X = lg[ractopamine]) (Fig. 3B). The limit of detection (LOD) was 20 pg/mL (LOD = 3S/M, S = 20, M = 2725), much more sensitive compared with that without the Gd-assisted amplification. There are two key factors affecting the sensitivity of eMRS: (1) Massive Gd^{3+} ions conjugated on the surface of MNPs can help enhance the T_2 signal because a proportion of the T_2 signal originates from Gd^{3+} ions. (2) The synergistic effect between MNPs and Gd^{3+} ions can contribute to an enhanced T_2 signal. Previous works have reported that the distance-dependent phenomenon could occur between a superparamagnetic quencher and a paramagnetic enhancer (Choi et al., 2017; Shin et al., 2018). The T_2 signal will be amplified based on the distance-dependent phenomenon. In this case, the T_2 signal of Gd^{3+}-MNPs may have a stronger T_2 signal than that of individual Gd^{3+}ion and MNPs if the distance-dependent amplification phenomenon occurs between Gd^{3+} ion and MNPs.

We also compared eMRS with the conventional ELISA in terms of the sensitivity (the LOD of ELISA was 576 pg/mL, LOD = 3S/M, S = 0.05, M = 0.26) (Fig. 3C and D). The LOD of eMRS improved about 25 folds compared with conventional ELISA that employd a colorimetric readout. Besides, the tedious washing steps in ELISA made it more complicated and laborious than eMRS. We compared the analytical performance of eMRS and conventional ELISA in Table S1, showing that the analytical time, sensitivity and operation of the eMRS were superior to those of conventional ELISA.

3.5. Selectivity and repeatability of eMRS

We further investigated the selectivity and repeatability of eMRS for the analysis of ractopamine. Using magnetic signals for readout, we could achieve good specificity for the detection of ractopamine where clenbuterol, salbutamol, chloramphenicol, and neomycin (10 ng/mL) acted as the interferents (Fig. S5). To study the recovery of eMRS, we added different amounts of ractopamine (from 0.1 to 100 ng/mL) into the blank swine urine samples and determined the concentration (Table S2). The recoveries were from 90% to 110% and the intra and inter-assay coefficients of variation (CV) were from 5.7% to 13.2%,. respectively. Both the recovery rate and relative standard deviations showed that this eMRS was reliable and was promising as a sensing technique for analyzing small molecules.

3.6. Real sample detection using eMRS

We applied eMRS to detect ractopamine in 20 swine urine samples to demonstrate its practical application. For comparison, we employed three methods including conventional ELISA, eMRS and high-performance liquid chromatography (HPLC)-mass spectrum (MS) to analyze these samples (Fig. 4A). For all the 20 samples, Sample 1, 3, 4, 7, 13–16, 18–20 were detected to be ractopamine-positive by both eMRS and HPLC-MS (Fig. 4B). In contrast, Sample 14–16 were detected to be ractopamine-negative by conventional ELISA because of its low sensitivity. The good correlation between eMRS and HPLC-MS suggested that eMRS had a good accuracy for small molecule detection such as ractopamine (Fig. 4C). Compared with conventional ELISA and HPLC-MS, eMRS could achieve a very high sensitivity without the need of any advanced instruments while conventional ELISA had a relatively low sensitivity and HPLC-MS required complicated equipment.

4. Conclusion

In summary, we report a multivalent magnetic sensing technique that enables magnetic separation and MRS by employing Gd^{3+}-nanoparticle as the probe. Gd^{3+} has a high binding ability with DOTA-MNPs with a number of 1.84×10^7 Gd^{3+} on one nanoparticle that can significantly amplify the T_2 signal for the MRS sensing. This multivalent eMRS sensing technique has a 25-fold enhancement in the detection sensitivity compared with conventional assays, and has been challenged with ractopamine detection in real samples. The exellent stability and high sensitivity make eMRS an attractive magnetic sensing tool for developing point-of-care biosensors. This eMRS sensing technique is currently incapable of high-throughput analysis, and we will address this issue in the future study by integrating other technologies such as the microfluidics or lab-on-chip technology.

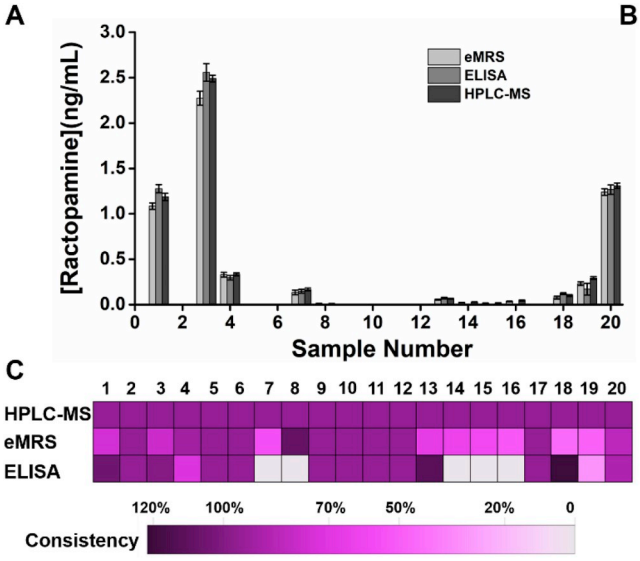

B

Samples	eMRS (ng/mL)	ELISA (ng/mL)	HPLC-MS (ng/mL)
1	1.08 ± 0.035	1.28±0.045	1.18±0.0404
2	0	0	0
3	2.27 ±0.078	2.55±0.097	2.49±0.0153
4	0.33±0.026	0.30±0.024	0.33±0.002
5	0	0	0
6	0	0	0
7	0.13±0.025	0.15±0.021	0.17±0.0153
8	0.01±0.002	0	0.01±0.0015
9	0	0	0
10	0	0	0
11	0	0	0
12	0	0	0
13	0.05±0.004	0.072±0.009	0.06±0.004
14	0.02±0.002	0	0.03±0.002
15	0.013±0.004	0	0.016±0.0027
16	0.04±0.003	0	0.045±0.006
17	0	0	0
18	0.08±0.015	0.12±0.01	0.099±0.01
19	0.23±0.02	0.17±0.066	0.29±0.015
20	1.24±0.036	1.27±0.05132	1.31±0.03

Fig. 4. Detection of ractopamine in swine urine samples. **(A)** Comparison of eMRS, conventional ELISA and HPLC-MS for the detection of ractopamine in swine urine samples; **(B)** Quantitative determinations of ractopamine in swine urine samples by eMRS, ELISA and HPLC-MS (n = 3). **(C)** The consistency between eMRS, conventional ELISA and HPLC-MS for the detection of ractopamine in swine urine samples. The error bars represent the standard deviation of three replicates (n = 3).

Declaration of competing interest

The authors declare that they have no known competing financial interests or personal relationships that could have appeared to influence the work reported in this paper.

CRediT authorship contribution statement

Yunlei Xianyu: Conceptualization, Formal analysis, Writing - original draft. **Yongzhen Dong:** Methodology, Investigation, Validation, Data curation. **Zhuo Zhang:** Data curation, Software, Visualization. **Zhanhui Wang:** Supervision, Writing - review & editing. **Wenbo Yu:** Writing - review & editing, Project administration. **Zhilong Wang:** Formal analysis, Supervision. **Yiping Chen:** Conceptualization, Methodology, Resources, Validation, Writing - review & editing, Funding acquisition.

Acknowledgements

We thank the Fundamental Research Funds for the Central Universities (2662019PY005) and the Beijing Nova Program (Z181100006218017) for financial support.

Appendix A. Supplementary data

Supplementary data to this article can be found online at https://doi.org/10.1016/j.bios.2020.112106.

The abbreviations list

MRS	Magnetic relaxation switching
MNPs	Magnetic nanoparticles
T_2	transverse relaxation time
T_1	longitudinal relaxation time
BSA-ractopamine	Complete antigen
HPLC-MS	High-performance liquid chromatography-mass spectrum
DOTA	1,4,7,10-tetraazacyclododecane-1,4,7,10-tetraacetic acid

References

Ananta, J.S., Godin, B., Sethi, R., Moriggi, L., Liu, X.W., Serda, R.E., Krishnamurthy, R., Muthupillai, R., Bolskar, R.D., Helm, L., Ferrari, M., Wilson, L.J., Decuzzi, P., 2010. Nat. Nanotechnol. 5 (11), 815–821.
Baynes, R.E., Dedonder, K., Kissell, L., Mzyk, D., Marmulak, T., Smith, G., Tell, L., Gehring, R., Davis, J., Riviere, J.E., 2016. Food Chem. Toxicol. 88, 112–122.
Bryant, L.H., Brechbiel, M.W., Wu, C.C., Bulte, J.W.M., Herynek, V., Frank, J.A., 1999. Jmri-J Magn. Reson. Im. 9 (2), 348–352.
Cao, L.M., Li, B.B., Yi, P.W., Zhang, H.L., Dai, J.W., Tan, B., Deng, Z.W., 2014. Biomaterials 35 (13), 4168–4174.
Caravan, P., 2006. Chem. Soc. Rev. 35 (6), 512–523.
Caravan, P., Ellison, J.J., McMurry, T.J., Lauffer, R.B., 1999. Chem. Rev. 99 (9), 2293–2352.
Chen, Y., Zou, M., Wang da, N., Li, Y., Xue, Q., Xie, M., Qi, C., 2013. Biosens. Bioelectron. 43, 6–11.
Chen, Y.P., Xianyu, Y.L., Wang, Y., Zhang, X.Q., Cha, R.T., Sun, J.S., Jiang, X.Y., 2015. ACS Nano 9 (3), 3184–3191.
Choi, J.S., Kim, S., Yoo, D., Shin, T.H., Kim, H., Gomes, M.D., Kim, S.H., Pines, A., Cheon, J., 2017. Nat. Mater. 16 (5), 537–542.
Chung, H.J., Castro, C.M., Im, H., Lee, H., Weissleder, R., 2013. Nat. Nanotechnol. 8 (5), 369–375.
De Leon-Rodriguez, L.M., Martins, A.F., Pinho, M.C., Rofsky, N.M., Sherry, A.D., 2015. J. Magn. Reson. Imag. 42 (3), 545–565.
Haun, J.B., Yoon, T.J., Lee, H., Weissleder, R., 2010. Wiley Interdiscip. Rev. : Nanomed. Nanobiotechnol. 2 (3), 291–304.
Huber, S., Min, C., Staat, C., Oh, J., Castro, C.M., Haase, A., Weissleder, R., Gleich, B., Lee, H., 2019. Biosens. Bioelectron. 126, 240–248.
Kang, T., Li, F., Baik, S., Shao, W., Ling, D., Hyeon, T., 2017. Biomaterials 136, 98–114.
Lei, Y.M., Xiao, B.Q., Liang, W.B., Chai, Y.Q., Yuan, R., Zhuo, Y., 2018. Biosens. Bioelectron. 109, 109–115.
Ma, W., Yin, H., Xu, L., Wang, L., Kuang, H., Xu, C., 2013. Chem. Commun. 49 (47), 5369–5371.
Marangoni, V.S., Neumann, O., Henderson, L., Kaffes, C.C., Zhang, H., Zhang, R.M., Bishnoi, S., Ayala-Orozco, C., Zucolotto, V., Bankson, J.A., Nordlander, P., Halas, N. J., 2017. Proc. Natl. Acad. Sci. U. S. A. 6960–6965.
Ni, D.L., Bu, W.B., Ehlerding, E.B., Cai, W.B., Shi, J.L., 2017. Chem. Soc. Rev. 46 (23), 7438–7468.
Rammohan, N., MacRenaris, K.W., Moore, L.K., Parigi, G., Mastarone, D.J., Manus, L.M., Lilley, L.M., Preslar, A.T., Waters, E.A., Filicko, A., Luchinat, C., Ho, D., Meade, T.J., 2016. Nano Lett. 16 (12), 7551–7564.
Rotz, M.W., Culver, K.S.B., Parigi, G., MacRenaris, K.W., Luchinat, C., Odom, T.W., Meade, T.J., 2015. ACS Nano 9 (3), 3385–3396.
Shao, H.L., Min, C., Issadore, D., Liong, M., Yoon, T.J., Weissleder, R., Lee, H., 2012. Theranostics 2 (1), 55–65.
Shin, T.H., Kang, S., Park, S., Choi, J.S., Kim, P.K., Cheon, J., 2018. Nat. Protoc. 13 (11), 2664–2684.
Srinivasan, S.Y., Paknikar, K.M., Gajbhiye, V., Bodas, D., 2018. ChemNanoMat 4 (2), 151–164.
Wang, W., Hao, C., Sun, M., Xu, L., Xu, C., Kuang, H., 2018b. Adv. Funct. Mater. 28 (22), 1800310 https://doi.org/10.1002/adfm.201800310.
Wang, Z., Carniato, F., Xie, Y.J., Huang, Y.R., Li, Y.W., He, S., Zang, N.Z., Rinehart, J.D., Botta, M., Gianneschi, N.C., 2017. Small 13 (43). https://doi.org/10.1002/smll.201701830. UNSP 1701830.
Wang, L., Lin, H., Chi, X., Sun, C., Huang, J., Tang, X., Chen, H., Luo, X., Yin, Z., Gao, J., 2018a. Small 14 (35), 1801612. https://doi.org/10.1002/smll.201801612.
Wu, J., Xianyu, Y.L., Wang, X.F., Hu, D.H., Zhao, Z.T., Lu, N., Xie, M.X., Lei, H.T., Chen, Y.P., 2018. Anal. Chem. 90 (7), 4725–4732.
Xianyu, Y.L., Wang, Q.L., Chen, Y.P., 2018. TrAC Trends Anal. Chem. (Reference Ed.) 106, 213–224.
Xiao, J., Zhang, G., Qian, J., Sun, X., Tian, J., Zhong, K., Cai, D., Wu, Z., 2018. ACS Appl. Mater. Interfaces 10 (8), 7003–7011.
Xu, Z., Kuang, H., Yan, W., Hao, C., Xing, C., Wu, X., Wang, L., Xu, C., 2012. Biosens. Bioelectron. 32 (1), 183–187.
Yang, L., Wang, Z., Ma, L., Li, A., Xin, J., Wei, R., Lin, H., Wang, R., Chen, Z., Gao, J., 2018. ACS Nano 12 (5), 4605–4614.
Zhang, W., Liu, L., Chen, H., Hu, K., Delahunty, I., Gao, S., Xie, J., 2018. Theranostics 8 (9), 2521–2548.
Zhang, Y., Zhou, D.J., 2012. Expert Rev. Mol. Diagn. 12 (6), 565–571.
Zhang, Z., Li, T., Sheng, Y., Liu, L., Wu, H.C., 2019. Small 15 (2), e1804078. https://doi.org/10.1002/smll.201804078.
Zhao, Y.W., Kuang, Y., Liu, M., Wang, J., Pei, R.J., 2018. Chem. Mater. 30 (21), 7511–7520.
Zheng, X.Y., Zhao, K., Tang, J., Wang, X.Y., Li, L.D., Chen, N.X., Wang, Y.J., Shi, S., Zhang, X., Malaisamy, S., Sun, L.D., Wang, X., Chen, C., Yan, C.H., 2017. ACS Nano 11 (4), 3642–3650.
Zhou, Z., Bai, R., Munasinghe, J., Shen, Z., Nie, L., Chen, X., 2017. ACS Nano 11 (6), 5227–5232.
Zhou, Z.J., Yang, L.J., Gao, J.H., Chen, X.Y., 2019. Adv. Mater. 31 (8), 1804567 https://doi.org/10.1002/adma.201804567.